Yuping Wan
Pingping Zhang
Zhenyu Huang
Lin Ji
Marko Jokić

https://doi.org/10.21278/TOF.41301
ISSN 1333-1124
eISSN 1849-1391

PARAMETER UNCERTAINTY EFFECTS OF STIFFENERS ON THE VIBRATION OF PLATES

Summary

The paper concerns parameter uncertainty effects of rib-stiffeners on the vibro-acoustics of thin plate structures. To gain a deep insight into the uncertainty propagation mechanism, a simple beam-stiffened plate model is built up in the first instance. By a simple mode-based hybrid technique, both the dynamic response of the beam and the statistical energy response of the plate can be approximated as functions of the beam natural frequency variations. It is found that if the amount of beam uncertainty is small enough (e.g., the generated set of natural frequency variations is narrower than the corresponding half-power bandwidth of the resonant modes), the real part of the beam mobility tends to be affected relatively little compared to the imaginary part. As a result, only the phase part of the dynamic response of the beam tends to be affected while the amplitude part can be affected relatively slightly. This is especially true when the beam and the plate have a large dynamic mismatch. One can thus deduce that, for stiffened-panel structures, the parameter uncertainties of stiffeners tend to affect little the structure-borne-sound transmission between ribs and the panel foundations. Numerical investigations of different rib-stiffened plates were conducted to validate the main conclusions.

Key words: *parameter uncertainty, mid-frequency vibration, beam-stiffened plates*

1. Introduction

Mid-frequency vibration is characterized by a simultaneous occurrence of both long- and short-wavelength deformations within the same model [1]. Typical examples are beam-stiffened plates, in which the beam components are usually very stiff with low modal density while the plates are very flexible with high modal density. When excited by external excitations, the system can exhibit significant mid-frequency behaviour in a quite large frequency range. Among the currently existing mid-frequency methods, the hybrid modelling technique is among the most widely used and well developed [2]. By describing the stiff components deterministically and the flexible ones statistically, the technique can provide a good compromise between the computational accuracy and efficiency. In recent years, the influence of subsystem parameter uncertainties on the mid-frequency vibration of built-up systems has drawn more and more attention from both academics and engineers [3], which

has resulted in a number of publications, e.g. [4-5]. However, the current investigations are found to be mainly on the uncertainty effects of the flexible components on the vibro-acoustics of the built-up systems, while the uncertainty effects of the stiff components still require more research efforts [6].

With the above in mind, a simple mode-based hybrid technique is employed to investigate the parameter uncertainty effects of rib/stiffeners on the mid-frequency vibro-acoustics of stiffened plates. A simple beam-stiffened plate model is set up in the first instance to gain a deep insight into the uncertainty propagation mechanism via the beam-plate coupling. Firstly, the mode-based approach is briefly reviewed in Section 2. Then the beam parameter uncertainty effects on both the displacement response of the beam and the power transmitted to the plate can be approximated in terms of the beam natural frequency variations in Section 3. Numerical examples are provided in Section 4 to illustrate the theoretical predictions, with the major conclusions being summarized in Section 5.

2. Dynamic analysis of a simple generic built-up system

A simple generic built-up structure is set up in the first instance, as shown in Fig. 1. The structure consists of only two subsystems, a and b , connected via a set of interface coordinates $\boldsymbol{\sigma}_{\mathbf{I}}$. If the model is excited by external force loadings at the local coordinates $\boldsymbol{\sigma}_{\mathbf{e}}$, the dynamic response of the built-up system can be predicted in an analytical way by a so-called "mode-based approach" in [7]. The main theoretical procedure of the approach can be briefly summarized as follows. For simplicity, the analysis assumes that both subsystems are uniform and homogeneous structures.

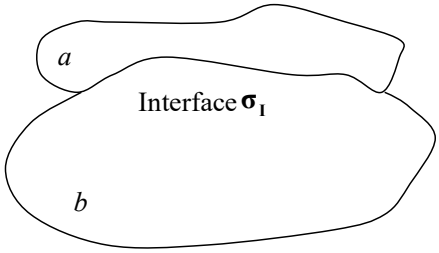

Fig. 1 A simple generic built-up structure

2.1 Dynamic modelling procedure of the mode-based technique

Step 1: modal analysis of each subsystem

Fig. 2 shows the force loadings of subsystem a for instance, where the external force loadings are represented by $F_e^{(a)}\left(\boldsymbol{\sigma}_{\mathbf{e}}\right)e^{i\omega t}$ while the resulting interface force distributions at $\boldsymbol{\sigma}_{\mathbf{I}}$ by $F_I^{(a)}\left(\boldsymbol{\sigma}_{\mathbf{I}}\right)e^{i\omega t}$. Here ω is the excitation frequency, and $i^2=-1$. Because of the linearity of the system, $e^{i\omega t}$ in both the excitation and the response terms have been omitted in the analysis.

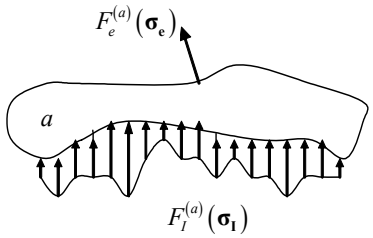

Fig. 2 Dynamic illustration of subsystem a

By modal analysis, the displacement of the subsystem in Fig. 2 can be expressed as

$$w^{(a)}\left(\boldsymbol{\sigma}\right)=\sum_{n} w_n^{(a)}\Phi_n^{(a)}\left(\boldsymbol{\sigma}\right) \tag{1}$$

where w_n is the nth generalized coordinate of the subsystem and Φ_n is the corresponding dimension-normalized mode shape function which satisfies the condition

$$\int_{V^{(a)}} \Phi_n^{(a)}\left(\boldsymbol{\sigma}^{(a)}\right)\Phi_{n'}^{(a)}\left(\boldsymbol{\sigma}^{(a)}\right)d\boldsymbol{\sigma}^{(a)}=\delta_{nn'} \tag{2}$$

Under the force loading condition shown in Fig. 2, $w_n^{(a)}$ can be determined by

$$w_n^{(a)}=Y_n^{(a)}\left(f_{\mathrm{e},n}^{(a)}+f_{\mathrm{I},n}^{(a)}\right) \tag{3}$$

where $Y_n^{(a)}$ is the nth modal receptance of the subsystem, while $f_{\mathrm{e},n}^{(a)}$ and $f_{\mathrm{I},n}^{(a)}$ are the nth modal forces corresponding to $F_e^{(a)}\left(\boldsymbol{\sigma}_{\mathbf{e}}\right)$ and $F_I^{(a)}\left(\boldsymbol{\sigma}_{\mathbf{I}}\right)$, respectively, given by

$$Y_n^{(a)}=\frac{1}{m_a'}\left[\frac{1}{\omega_n^{(a)2}\left(1+i\eta_n^{(a)}\right)-\omega^2}\right] \tag{4}$$

$$f_{\mathrm{e},n}^{(a)}=\int_{V_{\mathrm{e}}^{(a)}} F_{\mathrm{e}}^{(a)}\left(\boldsymbol{\sigma}_{\mathbf{e}}\right)\Phi_n^{(a)}\left(\boldsymbol{\sigma}_{\mathbf{e}}\right)d\boldsymbol{\sigma}_{\mathbf{e}} \tag{5}$$

$$f_{\mathrm{I},n}^{(a)}=\int_{V_{\mathrm{I}}^{(a)}} F_{\mathbf{I}}^{(a)}\left(\boldsymbol{\sigma}_{\mathbf{I}}\right)\Phi_n^{(a)}\left(\boldsymbol{\sigma}_{\mathbf{I}}\right)d\boldsymbol{\sigma}_{\mathbf{I}} \tag{6}$$

In the above equations, m_a', $\eta_n^{(a)}$ and $\omega_n^{(a)}$ are the mass distribution, the damping loss factor, and the nth natural frequency of subsystem a, respectively, while $V_{\mathrm{e}}^{(a)}$ and $V_{\mathrm{I}}^{(a)}$ represent the regions in which the external and interface force loadings act.

If a truncated set of modes is used, Eq. (3) can then be written in a matrix form as

$$\mathbf{w}_{\mathbf{n}}^{(a)}=\mathbf{Y}_{\mathbf{n}}^{(a)}\left(\mathbf{f}_{\mathbf{e,n}}^{(a)}+\mathbf{f}_{\mathbf{I,n}}^{(a)}\right) \tag{7}$$

where $\mathbf{w}_{\mathbf{n}}^{(a)}$, $\mathbf{f}_{\mathbf{e,n}}^{(a)}$ and $\mathbf{f}_{\mathbf{I,n}}^{(a)}$ are the column vectors composed of $w_n^{(a)}$, $f_{\mathrm{e},n}^{(a)}$ and $f_{\mathrm{I},n}^{(a)}$, respectively, while $\mathbf{Y}_{\mathbf{n}}^{(a)}$ is a diagonal matrix whose nth diagonal element is $Y_n^{(a)}$.

The above analytical procedures are also applicable to subsystem b by replacing the superscript (a) by (b).

Step 2: Interface decomposition

Assume that the interface force and displacement distributions $F_{\mathrm{I}}\left(\boldsymbol{\sigma}_{\mathbf{I}}\right)$ and $w_{\mathrm{I}}\left(\boldsymbol{\sigma}_{\mathbf{I}}\right)$ can be decomposed in terms of a set of complete basis functions $\mathrm{X}_k\left(\boldsymbol{\sigma}_{\mathbf{I}}\right)$ as

$$F_{\mathrm{I}}\left(\boldsymbol{\sigma}_{\mathbf{I}}\right)=\sum_{k} f_{\mathrm{I},k}\mathrm{X}_{\mathrm{I},k}\left(\boldsymbol{\sigma}_{\mathbf{I}}\right) \tag{8}$$

$$w_{\mathrm{I}}\left(\boldsymbol{\sigma}_{\mathbf{I}}\right)=\sum_{k} w_{\mathrm{I},k}\mathrm{X}_{\mathrm{I},k}\left(\boldsymbol{\sigma}_{\mathbf{I}}\right) \tag{9}$$

where, $f_{\mathrm{I},k}$ is the so-called kth generalized interface force, and $w_{\mathrm{I},k}$ is the kth generalized interface coordinate. Here $\mathrm{X}_{k}\left(\boldsymbol{\sigma}_{\mathbf{I}}\right)$ is orthogonal such that

$$\int_{V_{\mathrm{I}}} \mathrm{X}_{\mathrm{I},k}\left(\boldsymbol{\sigma}_{\mathbf{I}}\right)\mathrm{X}_{\mathrm{I},k'}\left(\boldsymbol{\sigma}_{\mathbf{I}}\right)d\boldsymbol{\sigma}_{\mathbf{I}}=\delta_{kk'} \tag{10}$$

From Eqs. (8) - (9), one can see that the physical coupling DOFs of the built-up structure have been transferred into generalized coupling DOFs. This DOF-transferring technique is potentially very useful for reducing the number of DOFs involved in the calculation by truncating the set of (infinite) basis functions into a convenient finite number.

Step 3: Impose the interface boundary condition on the set of basis functions

Let $\mathbf{T}_{\mathbf{I}}^{(a)}$ and $\mathbf{T}_{\mathbf{I}}^{(b)}$ represent the transformation matrices which relate the local coordinates of $\boldsymbol{\sigma}_{\mathbf{I}}^{(a)}$, $\boldsymbol{\sigma}_{\mathbf{I}}^{(b)}$ and $\boldsymbol{\sigma}_{\mathbf{I}}$ in the forms

$$\boldsymbol{\sigma}_{\mathbf{I}}^{(a)}=\mathbf{T}_{\mathbf{I}}^{(a)}\boldsymbol{\sigma}_{\mathbf{I}},\ \ \boldsymbol{\sigma}_{\mathbf{I}}^{(b)}=\mathbf{T}_{\mathbf{I}}^{(b)}\boldsymbol{\sigma}_{\mathbf{I}} \tag{11}$$

Both $\mathbf{T}_{\mathbf{I}}^{(a)}$ and $\mathbf{T}_{\mathbf{I}}^{(b)}$ are orthogonal matrices which satisfy $\mathbf{T}_{\mathbf{I}}^{(a)^{\mathrm{T}}}=\mathbf{T}_{\mathbf{I}}^{(a)^{-1}}$ and $\mathbf{T}_{\mathbf{I}}^{(b)^{\mathrm{T}}}=\mathbf{T}_{\mathbf{I}}^{(b)^{-1}}$, where the superscript T represents the matrix transpose. The boundary conditions along the interfaces give

$$F_{\mathrm{I}}\left(\boldsymbol{\sigma}_{\mathbf{I}}\right)=-F_{\mathrm{I}}^{(a)}\left(\boldsymbol{\sigma}_{\mathbf{I}}^{(a)}\right)=F_{\mathrm{I}}^{(b)}\left(\boldsymbol{\sigma}_{\mathbf{I}}^{(b)}\right) \tag{12}$$

$$w_{\mathrm{I}}\left(\boldsymbol{\sigma}_{\mathbf{I}}\right)=w^{(a)}\left(\boldsymbol{\sigma}_{\mathbf{I}}^{(a)}\right)=w^{(b)}\left(\boldsymbol{\sigma}_{\mathbf{I}}^{(b)}\right) \tag{13}$$

Substituting Eq. (8)-(9) into (12) and (13) gives

$$f_{\mathrm{I},n}^{(a)}=-\sum_{k} f_{\mathrm{I},k}\int_{V_{\mathrm{I}}^{(a)}} \Phi_{n}^{(a)}\left(\boldsymbol{\sigma}_{\mathbf{I}}^{(a)}\right)\mathrm{X}_{\mathrm{I},k}\left(\mathbf{T}_{\mathbf{s}}{}^{T}\boldsymbol{\sigma}_{\mathbf{I}}^{(a)}\right)d\boldsymbol{\sigma}_{\mathbf{I}}^{(a)} \tag{14}$$

For the truncated sets of $\Phi_{n}^{(a)}$ and X_{k}, Eq. (14) can be expressed in a matrix form as

$$\mathbf{f}_{\mathbf{I},\mathbf{n}}^{(a)}=-\boldsymbol{\alpha}_{\mathbf{I}}^{(a)}\mathbf{f}_{\mathbf{I},\mathbf{k}} \tag{15}$$

where $\mathbf{f}_{\mathbf{I},\mathbf{k}}$ is the column vector of $f_{I,k}$, and $\boldsymbol{\alpha}_{\mathbf{I}}^{(a)}$ is the $n\times k$ matrix, given by

$$\alpha_{\mathrm{I},nk}^{(a)}=\int_{V_{\mathrm{I}}^{(a)}} \Phi_{n}^{(a)}\left(\boldsymbol{\sigma}_{\mathbf{I}}^{(a)}\right)\mathrm{X}_{\mathrm{I},k}\left(\mathbf{T}_{\mathbf{I}}^{(a)\mathrm{T}}\boldsymbol{\sigma}_{\mathbf{I}}^{(a)}\right)d\boldsymbol{\sigma}_{\mathbf{I}}^{(a)} \tag{16}$$

$w_{n}^{(a)}$ can now be written, by Eq. (7), as

$$\mathbf{w}_{\mathbf{n}}^{(a)}=\mathbf{Y}_{\mathbf{n}}^{(a)}\left(\mathbf{f}_{\mathbf{e},\mathbf{n}}^{(a)}-\boldsymbol{\alpha}_{\mathbf{I}}^{(a)}\mathbf{f}_{\mathbf{I},\mathbf{k}}\right) \tag{17}$$

Similarly, for subsystem b, one can derive

$$\mathbf{w}_{\mathbf{m}}^{(b)} = \mathbf{Y}_{\mathbf{m}}^{(b)}\left(\mathbf{f}_{\mathbf{e,n}}^{(b)} + \boldsymbol{\alpha}_{\mathbf{I}}^{(b)}\mathbf{f}_{\mathbf{I,k}}\right) \tag{18}$$

Applying the displacement continuity boundary condition along the interface leads to

$$\boldsymbol{\alpha}_{\mathbf{I}}^{(a)\mathrm{T}}\mathbf{w}_{\mathbf{n}}^{(a)} = \boldsymbol{\alpha}_{\mathbf{I}}^{(b)\mathrm{T}}\mathbf{w}_{\mathbf{m}}^{(b)} = \mathbf{w}_{\mathbf{I,k}} \tag{19}$$

Combining Eq. (17) - (19), the interface force and displacement distributions can finally be obtained in terms of the generalized interface coordinates as

$$\mathbf{w}_{\mathbf{I,k}} = \mathbf{A}_{\mathbf{I}}^{(b)}\left[\mathbf{A}_{\mathbf{I}}^{(a)} + \mathbf{A}_{\mathbf{I}}^{(b)}\right]^{-1}\left(\boldsymbol{\alpha}_{\mathbf{I}}^{(a)\mathrm{T}}\mathbf{Y}_{\mathbf{n}}^{(a)}\mathbf{f}_{\mathbf{e,n}}^{(a)} - \boldsymbol{\alpha}_{\mathbf{I}}^{(b)\mathrm{T}}\mathbf{Y}_{\mathbf{m}}^{(b)}\mathbf{f}_{\mathbf{e,m}}^{(b)}\right) \tag{20}$$

$$\mathbf{f}_{\mathbf{I,k}} = \left[\mathbf{A}_{\mathbf{I}}^{(a)} + \mathbf{A}_{\mathbf{I}}^{(b)}\right]^{-1}\left(\boldsymbol{\alpha}_{\mathbf{I}}^{(a)\mathrm{T}}\mathbf{Y}_{\mathbf{n}}^{(a)}\mathbf{f}_{\mathbf{e,n}}^{(a)} - \boldsymbol{\alpha}_{\mathbf{I}}^{(b)\mathrm{T}}\mathbf{Y}_{\mathbf{m}}^{(b)}\mathbf{f}_{\mathbf{e,m}}^{(b)}\right) \tag{21}$$

where

$$\mathbf{A}_{\mathbf{I}}^{(a)} = \boldsymbol{\alpha}_{\mathbf{I}}^{(a)\mathrm{T}}\mathbf{Y}_{\mathbf{n}}^{(a)}\boldsymbol{\alpha}_{\mathbf{I}}^{(a)}, \quad \mathbf{A}_{\mathbf{I}}^{(b)} = \boldsymbol{\alpha}_{\mathbf{I}}^{(b)\mathrm{T}}\mathbf{Y}_{\mathbf{m}}^{(b)}\boldsymbol{\alpha}_{\mathbf{I}}^{(b)} \tag{22}$$

Physically, $\mathbf{A}_{\mathbf{I}}^{(a)}$ and $\mathbf{A}_{\mathbf{I}}^{(b)}$ provide the inter-modal couplings between subsystems a and b via the interface.

Step 4: Solve the vibration response of the built-up system

Following Eq. (20) - (21), the modal coordinates of subsystem a, after coupling with b, can then be finally obtained as

$$\begin{aligned}\mathbf{w}_{\mathbf{n}}^{(a)} = \mathbf{Y}_{\mathbf{n}}^{(a)}&\left[\mathbf{I} - \boldsymbol{\alpha}_{\mathbf{I}}^{(a)}\left[\mathbf{A}_{\mathbf{I}}^{(a)} + \mathbf{A}_{\mathbf{I}}^{(b)}\right]^{-1}\boldsymbol{\alpha}_{\mathbf{I}}^{(a)\mathrm{T}}\mathbf{Y}_{\mathbf{n}}^{(a)}\right]\mathbf{f}_{\mathbf{e,n}}^{(a)} \\ &+ \mathbf{Y}_{\mathbf{n}}^{(a)}\boldsymbol{\alpha}_{\mathbf{I}}^{(a)}\left[\mathbf{A}_{\mathbf{I}}^{(a)} + \mathbf{A}_{\mathbf{I}}^{(b)}\right]^{-1}\boldsymbol{\alpha}_{\mathbf{I}}^{(b)\mathrm{T}}\mathbf{Y}_{\mathbf{m}}^{(b)}\mathbf{f}_{\mathbf{e,m}}^{(b)}\end{aligned} \tag{23}$$

Similar expression can be obtained for $\mathbf{w}_{\mathbf{m}}^{(b)}$ (modal coordinates of subsystem b) by replacing the superscript (a) by (b) and (b) by (a) in Eq. (23).

The power transmitted between the two subsystems can finally be estimated by substituting Eq. (20) - (21) into

$$P_{\mathrm{tr}} = \frac{1}{2}\mathrm{Re}\left\{i\omega\sum_{k} w_{\mathrm{I},k} f_{\mathrm{I},k}^{*}\right\} \tag{24}$$

The above predicting procedures can be extended to built-up systems with more than two subsystem components straightforwardly as long as the corresponding matrices in Eq. (23) - (24) are extended properly.

2.2 Application to a simple beam-stiffened plate model

Assume that the system consists of a beam attached to a rectangular plate along a line parallel to the two opposite edges of the plate.

Let the beam modes be described as $\Phi_n^{(b)}\left(\mathbf{x}^{(b)}\right)$, and the plate modes along the interface line as $\Phi_m^{(p)}\left(\boldsymbol{\sigma}_{\mathrm{I}}^{(p)}\right)=\Psi_{m_x}^{(p)}\left(\mathbf{x}_{\mathbf{I}}^{(p)}\right)\Upsilon_{m_y}^{(p)}\left(\mathbf{y}_{\mathbf{I}}^{(p)}\right)$. If it is assumed that the plate has the same spatial variations along the coupling line as the beam, one may choose the set of beam modes as the interface basis functions, i.e.

$$\mathrm{X}_{\mathrm{I},n}\left(\mathbf{x}_{\mathbf{I}}\right)=\Phi_n^{(b)}\left(\mathbf{x}^{(b)}\right)=\Psi_n^{(p)}\left(\mathbf{x}_{\mathbf{I}}^{(p)}\right) \tag{25}$$

If the beam is assumed to be the source subsystem, by Eq. (16), one may obtain

$$\boldsymbol{\alpha}_{\mathbf{I}}^{(b)}=\mathbf{I};\quad \boldsymbol{\alpha}_{\mathbf{I}}^{(p)}=c_p\mathbf{I} \tag{26}$$

where c_p is a constant, given by

$$c_n^{(p)}=\left(\sum_{m_y}\Upsilon_{m_y}^{(p)}\left(\mathbf{y}_{\mathbf{I}}^{(p)}\right)\right) \tag{27}$$

The modal coordinates of the beam, by Eq. (23), can then be written in a simple form as

$$w_n^{(\mathrm{b})}=\frac{c_n^{(\mathrm{p})2}Y_n^{(\mathrm{p})}}{Y_n^{(\mathrm{b})}+c_n^{(\mathrm{p})2}Y_n^{(\mathrm{p})}}Y_n^{(\mathrm{b})}f_{e,n}^{(\mathrm{b})} \tag{28}$$

where

$$Y_n^{(p)}=\sum_{m_y}\frac{1}{\left(\omega_{n,m_y}^{(p)}\right)^2\left(1+i\eta_{n,m_y}^{(p)}\right)-\omega^2} \tag{29}$$

In this case, the corresponding interface modal force can be determined by

$$f_n^{(b)}=f_{\mathrm{I},n}=\frac{Y_n^{(b)}}{Y_n^{(b)}+c_n^{(p)2}Y_n^{(p)}}f_{e,n}^{(b)} \tag{30}$$

And the transmitted power from the beam to the plate, by Eq. (25), can finally be estimated as

$$P_{tr}=\frac{1}{2}\sum_n\left|\frac{Y_n^{(b)}}{Y_n^{(b)}+c_n^{(p)2}Y_n^{(p)}}\right|^2\mathrm{Re}\left\{i\omega\sum_n c_n^{(p)2}Y_n^{(p)}\right\}\left|f_{e,n}^{(b)}\right|^2 \tag{31}$$

Eq. (28) and (31) explicitly show how the dynamic response of the beam and the power transmitted to the plate can be affected by the dynamic properties of the beam and the plate subsystems. Therefore, in the following sections, Eq. (28) - (31) will be used to quantify the parameter uncertainty effects of the beam on the vibro-acoustics of beam-stiffened plates.

3. Parameter uncertainty effects of the stiff beam

3.1 Effects on the displacements of the beam

Assume that the parameter uncertainties of the stiff subsystem are represented by a set of known variations $\delta\omega_n$ around its normal natural frequency set ω_n. For a structure with a low mode count, it generally exists $\delta\omega_n << \Delta\omega_n=\omega_n\eta_n$ such that

$$\frac{\delta\omega_n}{\omega_n\eta_n} << 1 \tag{32}$$

In this case, Y_n in Eq. (4) can be modified as

$$Y_n' \approx \frac{1}{\omega_n^2\left(1+i\eta_n\right)-\omega^2+2\omega_n\delta\omega_n\left(1+i\eta_n\right)} \tag{33}$$

It is indicated by Eq. (33) that the influence of $\delta\omega_n$ tends to reach its maximum when ω tends to ω_n. Consequently, Eq. (33) can be simply approximated as

$$Y_n' \approx Y_n\left[\frac{1}{1+\frac{2\delta\omega_n}{\Delta\omega_n}\left(\eta_n-i\right)}\right] \tag{34}$$

Combined with Eq. (32), Eq. (34) is further reduced to

$$Y_n' \approx Y_n\left(1+i\frac{\delta\omega_n}{\Delta\omega_n}\right) \approx Y_n+\delta Y_n, \quad \delta Y_n = i\frac{\delta\omega_n}{\Delta\omega_n}Y_n \tag{35}$$

Substituting Eq. (35) into Eq. (28), the uncertainty effects of the stiff components on the vibrational response of the built-up system can be estimated in terms of $\delta\omega_n/\Delta\omega_n$ as

$$w_n^{(b)\prime} \approx \frac{c_r^2 Y_n^{(p)}}{Y_n^{(b)}+c_r^2 Y_n^{(p)}} Y_n^{(b)}\left(1+i\frac{\delta\omega_n}{\Delta\omega_n}\right) f_{e,n}^{(b)} = w_n^{(b)}\left(1+i\frac{\delta\omega_n^{(b)}}{\Delta\omega_n^{(b)}}\right) \tag{36}$$

Equations (35) and (36) have a very similar form which implies that the parameter uncertainty of the beam tends to affect the modal displacement of the coupled beam and the modal receptance of the uncoupled beam in a similar way. Moreover, the uncertainty effects are mainly produced on the imaginary parts as far as the beam input mobility terms are concerned. This suggests that the beam parameter uncertainty effects on the dynamic response of the beam are mainly on the phase parts, while the magnitudes of the dynamic response of the beam tend to be little affected.

3.2 Effects on the transmitted power to the plate

Substituting Eq. (35) into Eq. (31) yields

$$\begin{aligned} P_{tr}' \approx \frac{1}{2}\sum_n \left|\frac{Y_n^{(b)}}{Y_n^{(b)}+c_n^{(p)2}Y_n^{(p)}}\right|^2 \mathrm{Re}\left\{i\omega\sum_n c_n^{(p)2}Y_n^{(p)}\right\} \\ \times\left|f_{e,n}^{(b)}\right|^2\left[1+\left(\frac{\delta\omega_n^{(b)}}{\Delta\omega_n^{(b)}}\right)^2\right] \approx P_{tr}\left[1+\left(\frac{\delta\omega_n}{\Delta\omega_n}\right)^2\right] \end{aligned} \tag{37}$$

Comparing Eq. (37) with Eq. (36), one can deduce that the influence level of the beam uncertainty on the transmitted power, and hence the statistical energy response of the plate, tends to be relatively much lower than that on the dynamic response of the beam. In case $\delta\omega_n << \Delta\omega_n$, the influence of the beam uncertainty on the statistical response of the plate can be ignored.

It should be noted here that the parameter uncertainty of the plate was not involved during the analysis due to the independence of the beam and the plate parameter uncertainties.

The validity of the above theoretical conclusions can be illustrated by the numerical examples in the section below.

4. Numerical examples

4.1 Model descriptions

A set of numerical beam-stiffened plate models are built up, as shown in Fig. 3, where the beam component is assumed to be subjected to external force excitations. Although the system contains only a simple beam (stiff component) and a thin plate (flexible component), it enables the major features of uncertainty propagation within generic stiffened panel structures to be explicitly and efficiently highlighted.

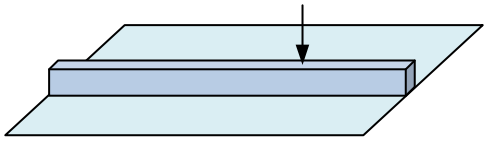

Fig. 3 Numerical model of the beam-stiffened plate

The beam has a length of $L_b = 2\,\mathrm{m}$ with a rectangular cross section of width (t_b) × height (h_b) = 0.03×0.04 m^2. A point, harmonic, unit force is located at a distance of $0.73\mathrm{m}$ from the right end of the beam. The plate is a rectangle with an area of length ($L_{x,p}$) × width ($L_{y,p}$) = 2×0.8 m^2. Both the beam and the plate are made of steel with Young's modulus of 2.1×10^{11} N/m^2, density of 7850 kg/m^3, Poisson's ratio of 0.3 and damping loss factor of 0.01.

The different dynamic mismatch conditions between the beam and the plate are achieved by varying the thicknesses of the plate. Two thicknesses are chosen: $h_p = 5\,\mathrm{mm}$ and $h_p = 2\,\mathrm{mm}$, which correspond to two wavelength ratios $\lambda_b/\lambda_p = 2.76$ and 4.37, respectively. Here, by the definition of flexural wavenumber and wavelength, $\lambda_b/\lambda_p \approx \sqrt{h_b/h_p}$.

The beam randomness is simulated by randomly varying its mass density within a range of $\pm 3\%$. In this case, the averaged natural frequency variation of the beam is only about a third of its averaged modal bandwidth up to the first 20 modes of the beam. Consequently, the condition of Eq. (32) can be considered as satisfied.

The variations of real and imaginary parts of the input mobility of the beam at the forcing point as well as the power transmitted to the plate can then be calculated based on either analytical or FE modelling, as appropriate.

In order to show clearly the uncertainty influential levels, a dimensionless variation ratio is defined as $\mathrm{E}\left[u - u_0\right]/u_0$; here, u is the response of interest, u_0 is the response corresponding to the nominal parametric values of the model, and $\mathrm{E}[\cdot]$ represents the ensemble average. The whole ensemble contains 20 samples whose mass densities are randomly distributed from $[-3\%, +3\%]$ around its nominal value.

4.2 Analytical modelling

In the first instance, both the beam and the plate in Fig. 3 are assumed to be simply supported so that an analytical modelling technique based on modal summation can be used.

Figure 4 shows a comparison between the variation ratios of the real and imaginary parts of the input mobility of the beam at the forcing point and that of the transmitted power from the beam to the plate when the plate thickness is 5 mm. It is shown that, as expected from Eq. (36) - (37), the beam parameter uncertainty effects are much more significant on the imaginary part of the beam mobility than those on the real part and on the transmitted power, especially at many resonances of the coupled system.

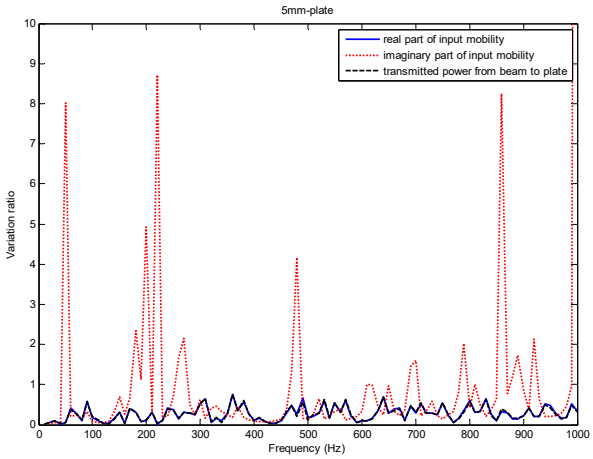

Fig. 4 Comparison of the variation ratios when the plate thickness is 5 mm

Figure 5 shows the relevant variation ratios when the plate thickness is 2 mm. When compared with the 5mm-plate coupling case, it is found that the beam parameter uncertainty influence on the imaginary part of the input mobility of the beam is actually stronger while the influence on the real part of beam mobility and the transmitted power is almost unchanged in both coupling cases.

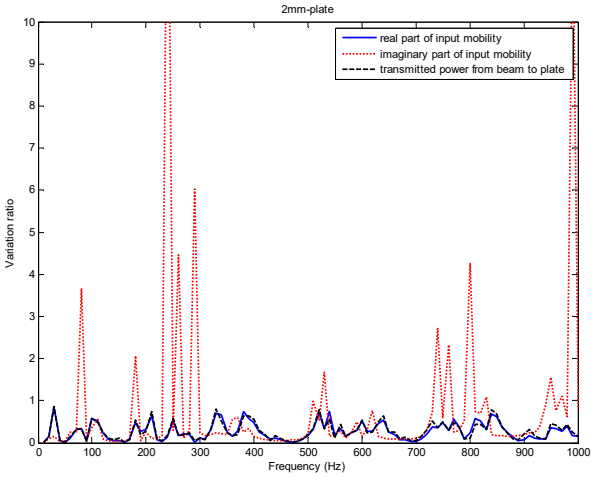

Fig. 5 Comparison of the variation ratios when the plate thickness is 2 mm.

In Fig. 5 one can see that the influence level of the parametric uncertainty of the beam on the imaginary part of the dynamic response of the beam increases as the large dynamic mismatch of the system increases.

Figures 4 and 5 are in very good agreement with the theoretical conclusions drawn from Section 3 (e.g., Eq. (35)-(37)). However, it should be noted that Eq. (35)-(37) will lose their validity for the frequency region where the plate possess very low modal density. In this case, the underlying theoretical assumption of Section 3 is not valid.

4.3 FE Modelling

To investigate the generic level of the theoretical conclusions drawn in Section 3, both the beam and the plate models in Fig. 3 are now assumed to be in fully-fixed boundaries, while the material properties of the beam/plate remain unchanged. In this case, FEM simulations done by the COMSOL Multiphysics software are employed to quantify the beam uncertainty effects by comparing the variation ratios of the different responses of the beam/plate system. During the calculation, the plate thickness employed was 5mm, and a tetrahedral mesh was used to model the beam and the plate with an element size of 30mm.

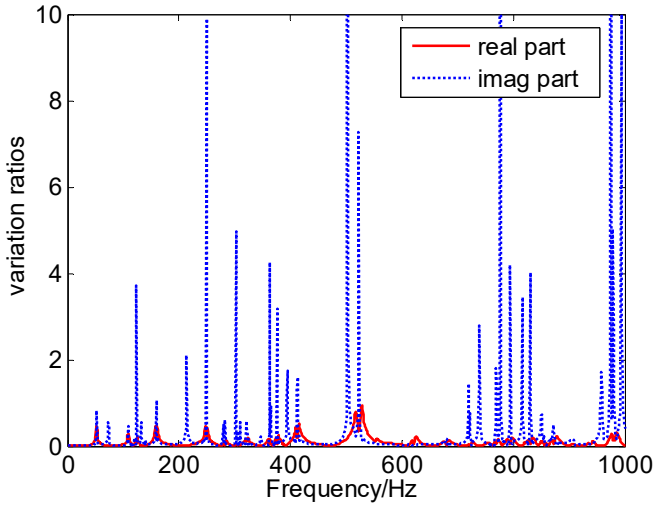

Fig. 6 Comparison of variation ratios of the real and imaginary parts of the input mobility of the beam at the forcing point for fully-fixed boundaries.

Figure 6 shows a comparison between the variation ratios of the real and imaginary parts of the input mobility. It can be seen that, similar to the simply supported boundary cases shown in Fig. 4-5, the real part of the input mobility of the beam tends to be affected relatively much less than the imaginary part.

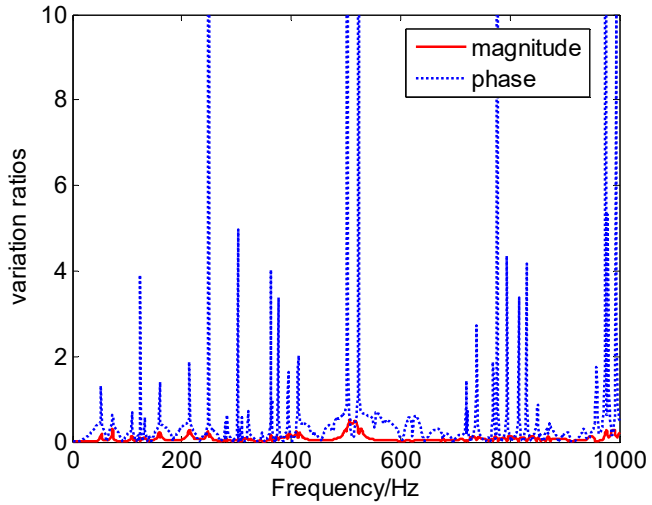

Fig. 7 Comparison of variation ratios of the magnitude and the phase of the input mobility of the beam at the forcing point for fully fixed boundaries.

In Fig. 7, the variation ratios of the magnitude and the phase of the input mobility are compared. As expected, it is seen from Fig. 7 that the beam parameter uncertainty does show relatively much less marked effects on the magnitude of the dynamic response than on the phase.

The above FE modelling results thus suggest that the theoretical derivations in Section 3 tend to be generic provided there is a relatively big dynamic mismatch between the beam and the plate.

Moreover, one may deduce from Fig. 6-7 that if the receiver structure in a generic source/receiver built-up system is relatively much more flexible than the source structure, the input power to the source can be simply treated as unaffected by the small parameter uncertainties of the source structure. Consequently, the statistical energy response of the receiver can be considered as being mainly affected by the parameter uncertainty of the receiver itself, while the source uncertainty effect can be neglected.

5. Concluding remarks

In the present research, a so-called “mode-based hybrid technique” is employed to investigate the parameter uncertainty effects of stiff components on the mid-frequency vibration behavior of built-up systems. A simple beam-stiffened plate model is set up; it assumes that the beam and the plate have the same spatial variations along the coupling line in the first instance. The beam parameter uncertainty effects on both the displacement response of the beam and the power transmitted to the plate are then analyzed in terms of the natural frequency variations of the stiff beam.

It is found that if the beam uncertainty is so small that the generated natural frequency variations are much narrower than a half power bandwidth of the resonant modes, then, the following conclusions can be made.

(1) The beam uncertainty tends to affect mainly the imaginary part of the beam dynamic response, while its real part is affected slightly , i.e., the beam response magnitude part tends to be relatively much less affected than its phase part by the beam uncertainties;

(2) As a result, one can deduce that the input power to the beam, and hence the transmitted power to the plate, tends to be affected by the beam uncertainties to a lesser degree;

(3) Consequently, one may expect that the statistical energy response of the plate tends to be affected mainly by the parameter uncertainty of the plate itself, while the beam uncertainty effect can be neglected.

The results in the present study can provide a certain level of simplification in predicting the structure-borne sound transmission within complex built-up systems when component parameter uncertainties need to be taken into account.

Acknowledgements

The study was sponsored by the National Natural Science Foundation of China (NSFC, Grant No. U1434201 and 51175300) and the State Key Laboratory of Vehicle NVH and Safety Technology of China (No. NVHSKL-201503).

REFERENCES

[1] Desmet W., 2002, Mid-frequency Vibro-Acoustic Modelling: Challenges and Potential Solutions, Proceedings of International Conference on Noise and Vibration Engineering (ISMA), Leuven, 835-862.

[2] Langley R. S., 2008, Recent Advances and Remaining Challenges in the Statistical Energy Analysis of Dynamic Systems. Proceedings of the 7th European Conference on Structural Dynamics, Southampton, UK.

[3] Mace B. R., Worden K., Manson G., 2005, Uncertainty in Structural Dynamics. Journal of Sound and Vibration, 288, 423-429. https://doi.org/10.1016/j.jsv.2005.07.014

[4] Manson G., 2007, Proceedings of the 1st International Conference on Uncertainty in Structural Dynamics, Sheffield: Sheffield University.

[5] Langley R. S., Cotoni V., 2007, Response Variance Prediction for Uncertain Vibro-Acoustic Systems Using a Hybrid Deterministic-Statistical Method. Journal of the Acoustical Society of America, 122, 3445-3463. https://doi.org/10.1121/1.2799499

[6] Cicirello A., Langley R. S., 2013, The Vibro-acoustic Analysis of Built-up Systems Using a Hybrid Method with Parametric and Non-Parametric Uncertainties. Journal of Sound and Vibration, 332, 2165-2178. https://doi.org/10.1016/j.jsv.2012.05.040

[7] Ji L., Mace B. R., Pinnington R. J., 2006, A Mode-based Approach for the Mid-Frequency Vibration Analysis of Coupled Long- and Short-Wavelength Structures. Journal of Sound and Vibration, 289, 148-170. https://doi.org/10.1016/j.jsv.2005.02.003

Submitted: 09.11.2016

Accepted: 06.02.2017

Yuping Wan
Changan Auto Global R&D Center,
Chongqing 401120, China
State Key Laboratory of Vehicle NVH and Safety Technology,
Chongqing 401120, China
Pingping Zhang
School of Mechanical Engineering,
Shandong University,
Jinan 250061, China
Zhenyu Huang
Institute of Intelligent Mechatronics Research, Shanghai Jiao Tong University,
Shanghai 200240,China
Lin Ji ✉
School of Mechanical Engineering,
Shandong University,
Jinan 250061, China
E-mail: *jilin@sdu.edu.cn*
Marko Jokić
Faculty of Mechanical Engineering and Naval Architecture, University of Zagreb,
Ivana Lučića 5, 10000 Zagreb, Croatia